Experimental Validation of Ex-Vessel Neutron Spectrum by Means of Dosimeter Materials Activation Method

S.A. Santa[*]

Center for Nuclear Reactor Technology and Safety, National Nuclear Energy Agency
Puspiptek Area, Serpong, Tangerang Selatan 15310, Indonesia

ARTICLE INFO

ABSTRACT

Neutron spectrum information in reactor core and around of ex-vessel reactor needs to be known with a certain degree of accuracy to support the development of fuels, materials, and other components. The most common method to determine neutron spectra is by utilizing the radioactivation of dosimeter materials. This report presents the evaluation of neutron flux incident on M3 dosimeter sets which were irradiated outside the reactor vessel, as well as the validation of neutron spectrum calculation. Al capsules containing both dosimeter set covered with Cd and dosimeter set without Cd cover have been irradiated during the 35th operational cycle in the M3 ex-vessel irradiation hole position 207 cm from core centerline at the space between the reactor vessel and the safety vessel. The capsules were positioned at Z = 0.0 cm of core midplane. Each dosimeter set consists of Co-Al, Sc, Fe, Np, Nb, Ni, B, and Ta. The gamma-ray spectra of irradiated dosimeter materials were measured by 63 cc HPGe solid-state detector and photo-peak spectra were analyzed using BOB75 code. The reaction rates of each dosimeter materials and its uncertainty were analyzed based on ^{59}Co (n,γ) ^{60}Co, ^{237}Np (n,f) ^{95}Zr-^{103}Ru, ^{45}Sc (n,γ) ^{46}Sc, ^{58}Fe (n,γ) ^{59}Fe, ^{181}Ta (n,γ) ^{182}Ta, and ^{58}Ni (n,p)^{58}Co reactions. The measured Cd ratios indicate that neutron spectrum at the irradiated dosimeter sets was dominated by low energy neutron. The experimental result shows that the calculated neutron spectra by DORT code at the ex-vessel positions need correction, especially in the fast neutron energy region, so as to obtain reasonable unfolding result consistent with the reaction rate measurement without any exception. Using biased DORT initial spectrum, the neutron spectrum and its integral quantity were unfolded by NEUPAC code. The result shows that total neutron flux, flux above 1.0 MeV, flux above 0.1 MeV, and the displacement rate of the dosimeter set not covered with Cd were 1.75×10^{12} n cm^2 s^{-1}, 1.83×10^8 n cm^2 s^{-1}, 2.94×10^{10} n cm^2 s^{-1}, and 2.39×10^{-11} dpa s^{-1}, respectively. The uncertainty of neutron flux by NEUPAC was mainly due to the error of the initial spectrum.

INTRODUCTION

Neutron energy characterization both in reactor core and in the vicinity of the reactor vessel is of a great importance for a large number of research activities involving neutron irradiation in nuclear reactors and neutron source facilities [1-7]. Precise knowledge of neutron energy spectrum is imperative to various fundamental and experimental studies in many field of nuclear physics, nuclear engineering and technology, medical sciences, and health physics research [8-16]. An accurate description of neutron spectrum is needed for understanding a reactor's characteristics and evaluating the quantity of neutron irradiation effect on reactor components such as fuel and materials [1,17-20].

The dosimeter material activation technique is a basic method for determination of neutron doses

[*]Corresponding author.
 E-mail address: santas@batan.go.id

internal to the reactor core and around reactor vessel [9,21,22], especially for the determination of neutron flux, the characteristics of neutrons in the core, and the characterizations of fuel, materials, and other components, as well as for reactor safety study [2,23-25]. The accuracy enhancement of neutron spectrum measurement is still a major issue in the reactor dosimetry research, in order to improve the accuracy of determination of the neutron spectrum, especially in reflector and reactor vessel area, and to verify the results of reactor surveilance program [26-31]. Balesteros *et al*. [26] suggested that there were 27 open issues that need to be addressed in reactor dosimetry. This experiment endeavors to solve two of those issues, *i.e*. developing a method to correlate between in-vessel and ex-vessel dosimetry data and understanding the potential interference caused by neutron interactions in accompanying elements that produce the same target radionuclide planned for use in retrospective dosimetry analysis.

In order to support postirradiation test analysis as well as surveillance test, neutron flux with spectral information should be evaluated accurately in the experimental fast reactor Joyo. Therefore a number of reactor dosimetry tests have been conducted at various locations, both in-core and ex-core, to assure the reliability and accuracy of the neutron dose for individual irradiation test.

This report presents the evaluation result of the dosimetry sets, which were irradiated in the M3 ex-vessel irradiation hole, 207 cm radial distance from the core centerline. The dosimeter sets were contained in an Al capsule, and each of the set was wrapped with 0.5 mm-thick Cd foil. Each dosimeter set consists of high-purity Fe, Ni, Ta, Nb, Co-Al, Np, Sc, and B. Using a stainless steel wire, the capsules were positioned in Z=0.0 mm from core midplane. Irradiated dosimeter materials were measured by means of gamma-ray spectrometry to estimate their reaction rate value. The measured reaction rates were compared with calculated values by NEUPAC. The contribution of thermal neutron flux to the total neutron flux was estimated from the measured Cd ratio.

The thermal neutron flux information is important in predicting thermal neutron damage effect to the materials by indirect mechanisms. Such mechanisms are correlated with the atomic displacement produced by atomic recoil following the thermal neutron absorption and the emission of a capture gamma ray [32,33]. By direct neutron collision, however, the thermal neutrons are not

generally capable of producing radiation damage in materials. Furthermore, the thermal neutron flux information is needed for correction of the fast neutron flux measurement, due to the presence of interfering radioactivities from dosimeter materials, for instance, from impurities that are subsequently activated by thermal neutrons, resulting in the same radionuclides as the ones to be measured. If the radioisotope to be measured is a fision product, disturbances in measurement can also be caused by the transmutation loss of higher actinides, or burnup of the fission product due to the thermal neutron absorption by the fission product. If the fast neutron flux is estimated solely from the activity of the chosen radioisotope, the estimate will not be accurate. The thermal neutron flux information is also necessary in predicting the radioactivity of reactor component. This report describes the experimental method, analysis of measured reaction rate, and evaluation of neutron flux at the M3 irradiation hole position of Joyo.

EXPERIMENTAL METHODS

Figure 1 illustrates the evaluation system used to validate the neutron spectrum outside of the reactor vessel.
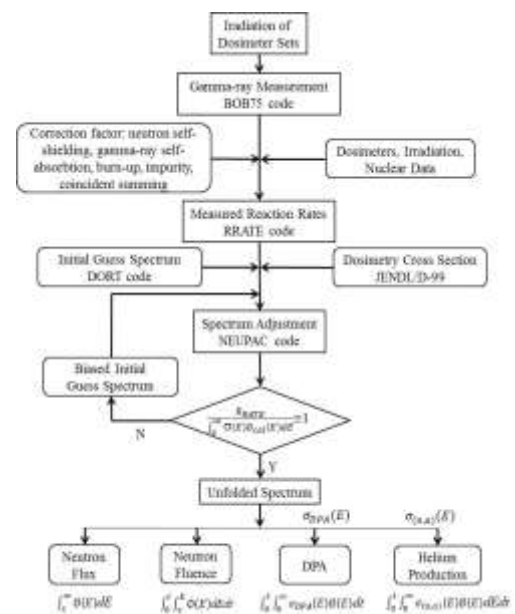

Fig. 1. Experimental validation procedure of ex-vessel neutron spectrum adjustment.

Dosimeter material and irradiation condition

The dosimeter sets were irradiated in the M3 irradiation hole, which is located in space

between the reactor vessel and the safety vessel. Figure 2 shows the irradiation position of dosimeter sets and capsules arrangement. Two dosimeter sets were contained in 35 mm-diameter and 95 mm-long Al capsules. Using the stainless steel wire, the dosimeter capsule was located in the M3 manhole in the level of Z=0.0 mm from core midplane. Each dosimeter set consists of high-purity Fe, Ni, Ta, Nb, Co-Al, Np, Sc, and B materials. The first dosimeter set was covered with 0.5 mm-thick Cd, and the second dosimeter set was covered with Al foil. Then, both dosimeter sets were wrapped with Al foils separately and loaded in 6 mm-thick Al capsule. Dosimeter weight, size, and purity data are tabulated in Table 1 and Table 2, respectively. The impurity materials of each dosimeter based on its Material Data Sheets have been confirmed by separated testing.
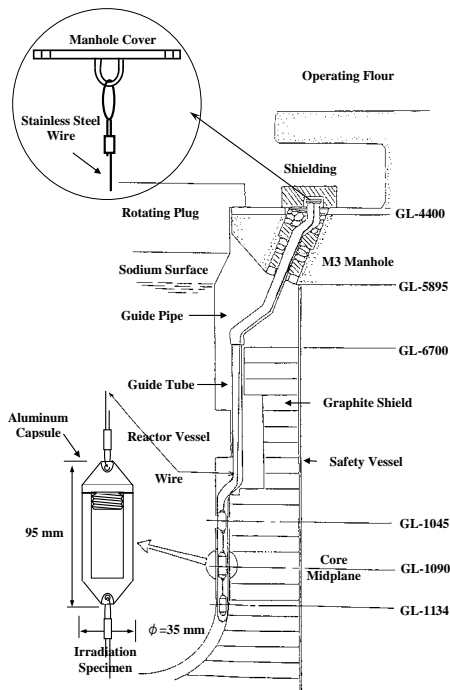

Fig. 2. Ex-vessel irradiation position and capsule arrangement.

Table 1. Dosimeter weight

Dosimeter Set Cd Covered[1]	Dosimeter weight[2] (mg)					Dosimeter weight[3] (mg)			
	Fe	Ni	Ta	Nb	Co-Al	Np	Sc	B	Blank
No	290	133	0.0612	10.4	2.87	2.013	0.101	0.122	43.4
Yes	304	138	0.0626	10.6	2.97	2.072	0.109	0.090	-

Note:
1) The Cd cover thickness is 0.5 mm
2) Weight error of all dosimeter materials (1σ %) are less than 0.1 % except for Ta less than 0.9 %
3) Encapsulated by vanadium capsule of 0.310 mm thickness

Table 2. Dosimeters' data and their purity

Dosimeter Mat.	Dosimeter Form	Size (mm) (ϕ x L)	Dosimeter Purity	Dosimeter Mat.	Dosimeter Form	Size (ϕ x L) (mm)	Detector Purity
Fe	Wire	2x12	0.999986	Np	Wire	1.5 x 8	Np (88.34wt % - ^{237}Np>0.99999
Ni	Wire	2x5	0.999976	Sc	Wire	1.5 x 8	Sc-MgO (1.55wt %-^{45}Sc)
Nb	Wire	0.5 6	0.9996150	B	Wire	1.27 x 8	B (93.04 at. %-^{10}B)
Co-Al	Wire	0.381x6	99/95 %	Blank	Wire	1.27 x 8	-
Ta	Foil[1]	1x3x0.0015[2]	0.999	Co-Al	Foil	0.38 x 6	0.46wt % - Co

Note:
1) The Ta foil is too small to be handled, so was put in Al tube.
2) The size of Ta foil : width × length × thickness

The dosimeter sets' irradiation was performed during the 35th operational cycle of Joyo MK II core. The core had accumulated 4,819 MWd at 100 MWt rated power with an effective irradiation time of 4.16×10^6 second. The reactor power history of the 35th duty cycle is shown in Fig. 3. The dosimeter sets were then discharged after several days to fulfill appropriate radiation dose rate for handing reasons.
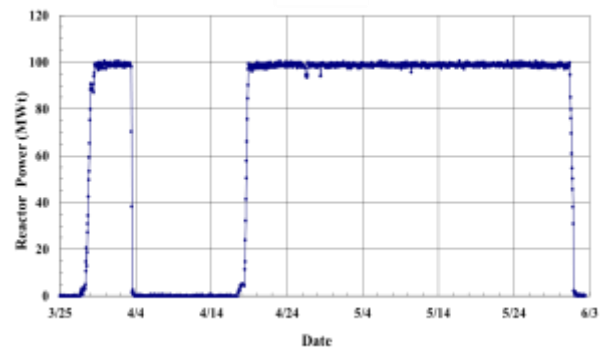

Fig. 3. Irradiation history of dosimeter set at the 35th cycle of Joyo MK-II core.

Neutron flux information

The neutron flux distribution across the Joyo MK-II core was calculated by the MAGI core management code system, based on diffusion theory with seven neutron energy groups. The original MAGI used the JFS-2 cross section set and now it has been updated to the JFS-3-J2 (JAERI Fast Set Version 3) set based on the JENDL-2 library [34]. The core configuration was modeled in the three-dimensional Hex-Z geometry for each operational cycle.

At positions away from the core, such as the M3 manhole, MAGI calculation may have a large uncertainty of neutron flux due to its high gradient and significant spectral change [35]. In the ex-core position, therefore, the transport calculation using DORT code is applied. This code calculates the neutron flux distribution in two-dimensional

discrete ordinate type R-Z or X-Y geometry using the neutron source distribution calculated by MAGI code. The group constant is structured to 103 energy groups.

Gamma ray measurement

To evaluate reaction rates, the irradiated dosimeters were measured by means of gamma-ray spectrometry using a 63-cc high-purity coaxial Ge solid-state detector system. The detector was calibrated using standard gamma-ray sources whose energies spanned those of the activated nuclides, from 80.998 keV of ^{133}Ba through 1836.063 keV of ^{88}Y standards. The accuracy of the gamma-ray measurement system was confirmed to be within 3 % through integral tests in the fast neutron spectrum fields in the Yayoi fast neutron source reactor at University of Tokyo and the reactor dosimetry intercomparison study between Joyo and EBR-II [34]. In order to measure gamma ray with appropriate accuracy, the gamma ray spectrum measurements were carried out at standard Ge detector to radiation source distances of 12, 28, 100, and 300 cm, depending on its activity.

The shift of calibration energy and gamma ray peak efficiency due to environmental change during experiment was verified by measuring ^{60}Co, ^{137}Cs, ^{133}Ba, and ^{152}Eu standard sources following each step for dosimeter sources measurement. The first and second measurement was conducted to identify the type of dosimeter materials and to determine its radiation dose levels. Using obtained radiation dose level, each dosimeter was then measured at its appropriate distance and counting time. The gamma ray spectra of the dosimeters were measured using the gamma-ray spectrometer and then analyzed using BOB75 code. This code can provide gamma ray spectrum, identify observed each photo-peak, determine the peak energy based on input calibration data, and calculate each observed peak area and its error. All those data are contained in the BOB75 output results.

Reaction rate evaluation

The specific activity, A_C, at the end of irradiation and reaction rates, R_{RATE}, were calculated using the following equation [36]:

$$A_C = \frac{\lambda C_P e^{\lambda T_c}}{\varepsilon_P P_\gamma W F_{SG} F_{SN} F_C \left(1 - e^{-\lambda T_m}\right)} \tag{1}$$

$$R_{RATE} = \frac{\lambda C_P A \left(e^{\lambda T_c}\right)}{\varepsilon_P P_\gamma W N_A pa F_{SG} F_{SN} F_C F_I F_B \left(1 - e^{-\lambda T_m}\right) S} \tag{2}$$

with S value given by

$$S = \frac{\lambda}{P_O} \int_0^T P(t) e^{-\lambda(T_I - t)} dt \tag{3}$$

where A_C is the specific dosimeter activity at the end of irradiation (Bq g^{-1}), R_{RATE} is the neutron reaction rate (reactions s^{-1} atom^{-1} (100 MWt)$^{-1}$), C_P is the corrected gamma-ray photo-peak area (count), ε_P is the detector counting efficiency for the point of sources, P_γ is the gamma ray emission probability, W is the dosimeter weight (g), p is the purity of dosimeter material, N_A is the Avogadro number, A is the atomic mass (amu), a is the isotopic abundance, T_i is the irradiation time (s), T_m is the real counting time (s), T_C is the time between the end of irradiation and the start of counting (s), F_B is the correction factor for burnup of dosimeter material, F_{SG} is the correction factor for gamma-ray self-absorption, F_{SN} is the correction factor for neutron self-shielding, F_C is the correction factor for random summing of gamma-ray counting, F_I is the correction factor for impurity of dosimeter material, λ is τηε decay constant of the radioisotope (s^{-1}), P_O is the nominal thermal power (MWt), and $P(t)$ is the time-dependent reactor power (MWt).

The saturation factor S can be determined from equation (4):

$$S = \frac{\lambda}{P_O} \sum_i P(t_i)(t_{i+1} - t_i) e^{-\lambda(T_i - t_j)}$$

$$S = \frac{\lambda}{P_O} \sum_i \left[P_I(t_{i+1}) - P_I(t_i)\right] e^{-\lambda(T_I - t_j)} \tag{4}$$

where $t_j = (t_{i+1} + t_i)/2$ and P_I is integrated power. The values of P_I were taken from the reactor online acquisition data.

The final reaction rate error is the sum of systematic error and random error and is expressed as follows:

$$\Delta R_{RATE_i} = \sum_1^K S_{i_K} + R_i \tag{5}$$

$$\overline{\Delta R_{RATE_i} \Delta R_{RATE_j}} = \sum_1^K S_{i_K} S_{j_K} + R_i R_j \delta_{ij} \tag{6}$$

where S is systematic error, R is random error, and δ_{ij} is the Kronecker delta.

Meanwhile the variance can be calculated using equation (7).

$$\left(\frac{\Delta R_{RATEi}}{R_{RATEi}}\right)^2 = \left(\frac{\Delta C_P}{C_P}\right)^2 + \left(\frac{\Delta A}{A}\right)^2 + \left(\frac{\Delta P_\gamma}{P_\gamma}\right)^2 + \left(\frac{\Delta W}{W}\right)^2 + \left(\frac{\Delta a}{a}\right)^2 + \left(\frac{\Delta p}{p}\right)^2 + \left(\frac{\Delta \varepsilon_P}{\varepsilon_P}\right)^2 +$$
$$\left(\frac{\Delta S}{S}\right)^2 + \left[\left(1 - \lambda T_C - \frac{\lambda T_M}{\left(e^{\lambda T_M} - 1\right)}\right)\left(\frac{\Delta T_{1/2}}{T_{1/2}}\right)\right]^2 + \left[\left(\frac{\lambda T}{\left(e^{\lambda T} - 1\right)} - \lambda T\right)\left(\frac{\Delta T_{1/2}}{T_{1/2}}\right)\right]^2 +$$
$$\left(\frac{\Delta L}{L}\right)^2 + \left[\left(\frac{\lambda T_M}{\left(e^{\lambda T_M} - 1\right)}\right)\left(\frac{\Delta T_M}{T_M}\right)\right]^2 + \left[\left(\lambda T_C\right)\left(\frac{\Delta T_C}{T_C}\right)\right]^2 \qquad (7)$$

Furthermore the covariance can be calculated using equation (8).

$$\overline{\left(\frac{\Delta R_i \Delta R_j}{R_i R_j}\right)} = \overline{\left(\frac{\Delta W_i \Delta W_j}{W_i W_j}\right)} + \overline{\left(\frac{\Delta \varepsilon_{Pi} \Delta \varepsilon_{Pj}}{\varepsilon_{Pi} \varepsilon_{Pj}}\right)} + \overline{\left(\frac{\Delta S_i \Delta S_j}{S_i S_j}\right)} + \overline{\left(\frac{\Delta L_i \Delta L_j}{L_i L_j}\right)} \quad (8)$$

The uncertainties of the dosimeter sources' positioning during the counting process were taken as two a half times the smallest meter scale, as shown in the following expression:

$$\Delta L = \frac{2\Delta M}{M}$$

where ΔM is 0.05 cm, and M is the distance between the dosimeter source and the HPGe detector. The uncertainty of the half-life is shown by the following equation:

$$\Delta \lambda = -\frac{\ln 2}{\left(T_{1/2}\right)^2} \Delta_{T_{1/2}}$$

The reaction rate formulation above was implemented by the RRATE code which needs to be calculated separately. In order tas followso achieve an appropriate measurement accuracy, some correction factors were considered, as given in subsections A-E as follows [36]:

Neutron Self-shielding Correction

The neutron self-shielding occurs when high cross-section atoms of the outer layer of the dosimeter reduce the neutron flux to the point where it significantly affects the activation of the inner atoms of the materials [37,38]. This is actually true of materials with high thermal cross-sections and essentially for resonance detectors. This can be minimized by using low weight percentage alloys such as Co-Al which is used in this experiment. The neutron self-shielding factor is not significant in the fast region where the cross-sections are relatively low. However, in the thermal and resonance region it would be more significant; therefore, thermal and resonance detectors should be as thin as possible. The self-shielding correction factor was calculated by the following analytical formulas [39]:

for a slab

$$F_{SN} = 1 - \frac{\xi}{2}\left(0.9228 + \ln\frac{1}{\xi}\right) \qquad \xi = \Sigma_a t \qquad (9)$$

for a cylinder

$$F_{SN} = 1 - \frac{4}{3}\xi \qquad \xi = \Sigma_a r \qquad (10)$$

In general, the value of $\xi = \frac{2}{surface \; area}\frac{volume}{}\Sigma_a$,

where Σ_a is the macroscopic neutron cross-section, t is the thickness of the slab, and r is the radius of the dosimeter material.

Gamma Ray Self-Absorption Correction

Gamma ray self-absorbtion may be observed during the counting of radiometric dosimeters, especially if the radiation of interest is a low-energy gamma ray or X-ray. It would again be desirable to use thin dosimeters in case the count rate is affected by dosimeter thickness.

By assuming that the response of detector is proportional to the gamma ray intensity and independent of photon energy, and that the distance between detector and dosimeter source is large compared with the dimension of the source, a good approximation for gamma ray self-absorption is given by [40]:

$$F_{SG} = e^{-\frac{8}{3\pi}\mu_a R} \qquad (11)$$

where μ_a is the linear absorption (cm^{-1}) of gamma ray intensity at its energy and R is the radius of the dosimeter wire materials (cm), respectively. Using the Taylor expansion formula, the gamma ray self-absorption correction above can be approached by the first order approximation as follows [36]:

$$F_{SG} = \left(1 - \frac{8}{3\pi}\mu_a R\right) \qquad (12)$$

For the dosimeter that was encapsulated by a vanadium capsule, the gamma ray self-absorption was formulated as follows:

$$F_{SG} = e^{-\mu_a t} \qquad (13)$$

where t is the thickness of the vanadium capsule. The formula above is also valid also for the Ta-foil dosimeter. The linear absorption coefficient was calculated from two data points of linear absorption [10] using log-log interpolation as follows:

$$\ln \mu = \frac{1}{\ln\left(\frac{E_2}{E_1}\right)}\left[\ln\left(\frac{E}{E1}\right)\ln \mu_2 + \ln\left(\frac{E_2}{E_1}\right)\ln \mu_1\right]. \quad (14)$$

Burnup Correction

The dosimeter material and its daughter nuclides are subject to burnup during the neutron irradiation. Therefore, the burnup effect must be corrected. The burnup correction factor, F_B, for Co, Ni, Sc, Fe, and Ta dosimeters were calculated as the ratio of dosimeter activity calculated by conventional formula represented in equation (15)

$$A_C = \frac{W N_A \sigma \phi}{A}\left(1 - e^{\lambda t}\right) \quad (15)$$

to the corresponding dosimeter activity calculated by ORIGEN2 code.

The burnup correction factor of ^{237}Np (n,f) should be calculated by considering the fission reactions of higher actinides that have an effect on burn-in to the fission product interest, such as the ^{137}Cs production chain from ^{237}Np (n,f) reaction.

Impurity Correction

The gamma rays from the reaction products are measured. At the same time, gamma rays from impurity elements are also measured. Therefore, the gamma ray counting rate from competing processes must be eliminated. The correction due to the impurity of dosimeter material can be anticipated if the trace impurity elements in dosimeter material are known. The information on dosimeter material impurities is listed in its Certificate of Nuclear Data Sheet. The gamma ray peak area from the competitor reactions can be eliminated by reducing the total peak area of interest with the peak area contributed by the impurity reactions.

Random Coincident Summing Correction

Random coincident summing occurs when measuring the high dose-irradiated dosimeter material under a small source-to-detector distance and a high-angle geometry during counting [41,42]. This effect can be neglected since all dosimeter materials were very small and the gamma ray measurements were carried out in appropriate radiation dose rates and at sufficient source to detector distances.

Neutron spectrum unfolding

The measurement of radioactivity induced by neutrons provides information of the neutron flux. Using a dosimeter set in which each dosimeter material has a different energy sensitivity, the information about the energy-dependent flux distribution can be obtained. Utilizing a set of measured reaction rates, the neutron spectrum can be estimated by solving the general equation (16):

$$R_{RATE_i} \pm \Delta R_{RATE_i} = \int_i (\sigma_i(E) \pm \Delta\sigma_i(E))\phi(E)d(E) \quad (16)$$

where $R_{RATE_i} \pm \Delta R_{RATE_i}$ are the measured reaction rate of the ith type of dosimeter material and the rate's corresponding error, and $\sigma_i(E) \pm \Delta\sigma_i(E)$ are the material's response function and its covariance, and $\phi(E)$ is the estimated spectrum.

The neutron spectrum at dosimeter sets' irradiation position was adjusted by measured reaction rates by solve the equation above, using the J1log-type of unfolding NEUPAC code. This code uses 103-group cross-section with error covariance processed from JENDL dosimetry file 99 (JENDL/D99) [43]. NEUPAC provides estimated neutron spectra, their integral quantities, and their sensitivities, including the error of unfolded spectra and integral quantities. PAC provides estimated neutron spectra and their integral quantities and sensitivities, as well as the errors of unfolded spectra and their integral quantities. The NEUPAC code also performs chi-square test on both input and output data.

RESULTS AND DISCUSSION

Gamma ray spectrum

The gamma rays from irradiated dosimeters were measured using high purity Germanium (Ge) gamma-ray detector. The measurements were conducted after 82-144 days of cooling time to obtain appropriate dose rates for the gamma ray counting system. The result of gamma ray spectra measument are follows. The gamma ray spectra of all the irradiated Co dosimeter show sharp photopeaks of 1173.24 keV and 1332.54 keV of ^{60}Co. The spectra of ^{237}Np (n,f) show clear photopeaks of 724.23 keV and 757.74 keV, both of ^{95}Zr, and 497.08 keV of ^{103}Ru among the complex photopeaks of various fission products. The 1596.5 keV photopeak of ^{140}Ba-^{140}La was also

detected but had an error of greater than 1 %, so it was not considered as the radioactive monitor. Other common fission product monitors such as the 661.6 keV of ^{137}Cs ($T_{1/2}$ = 30.17 y) and 133.5 keV of ^{144}Ce ($T_{1/2}$ = 284.89 d) did not appear clearly in the gamma ray spectra since the dosimeter set was irradiated for only a short period.

The photopeaks of 889.25 keV and 1120.52 keV of ^{45}Sc (n,γ) ^{46}Sc are observed clearly when it was measured 10 ks at 100 cm distance. The photopeak of 1121.28 keV and 1221.28 keV of ^{181}Ta (n,γ) ^{182}Ta were also shown clearly between other photopeaks of higher energies. The irradiated Ta dosimeters were measured for 10 ks at 100 cm distance. The gamma ray spectrum of Fe dosimeters were measured at 20 cm distance and 5 ks of counting time and it showed very sharp photopeaks of 1099.22 keV and 1299.56 keV. Ni dosimeter, at first, was measured at 12 cm distance for 5 ks, but the results showed a low counting rate. Therefore, Ni dosimeters were remeasured for 20 ks. The 810.75 keV photopeak of ^{58}Co radioisotope produced from ^{58}Ni (n,p) reaction showed the smallest activity compared to the other activated dosimeter materials. The gamma ray spectrum of Ni dosimeter shows several photopeaks of impurities but they do not disturb the photopeak of interest.

Table 3. Result of gamma ray photopeak counting of dosimeter sets

Dosimeter Sets	Reaction Type	Distance (cm)	Counting Time (ks)	Energy Peak (keV)	Peak Area (count)	Standard Deviation (%)
	^{59}Co(n,γ)^{60}Co	28	5	1173.210	147570	0.35
				1332.470	218656	0.22
	^{237}Np(n,f)^{95}Zr	12	20	724.230	80707	0.56
				756.740	95298	0.49
Dosimeter Set Without Cd cover	^{237}Np(n,f)^{103}Ru	12	20	497.080	176081	0.34
	^{45}Sc (n,γ) ^{46}Sc	100	10	889.251	235993	0.22
				1120.516	193819	0.23
	^{58}Fe(n,γ)^{59}Fe	28	5	1099.224	154466	0.27
				1291.563	100647	0.32
	^{58}Ni(n,p)^{58}Co	12	20	810.752	15338	0.99
	^{181}Ta(n,γ)^{182}Ta	100	10	1121.280	140511	0.28
				1221.418	102054	0.32
	^{59}Co(n,γ)^{60}Co	28	5	1173.210	133025	0.29
				1332.470	117830	0.29
	^{237}Np(n,f)^{95}Zr	12	20	724.230	69831	0.59
				756.740	82690	0.53
Dosimeter Set With Cd Cover	^{237}Np(n,f)^{103}Ru	12	20	497.080	151098	0.36
	^{45}Sc (n,γ) ^{46}Sc	100	10	889.251	52201	0.47
				1120.516	44890	0.48
	^{58}Fe(n,γ)^{59}Fe	28	5	1099.224	54911	0.44
				1291.563	35647	0.31
	^{58}Ni(n,p)^{58}Co	12	20	810.752	16015	0.94
	^{181}Ta(n,γ)^{182}Ta	100	10	1121.280	139117	0.28
				1221.418	100405	0.32

The radioactivity of minor impurity elements will not disturb the dosimeter's photopeaks of interest because the dosimeters were made of high-purity materials, and the trace element of each dosimeter material was not detected. Measured radioactivities of irradiated dosimeters from the dosimeter set with Cd foil cover removed and the dosimeters set with Cd foil cover on were analyzed using BOB75 gamma ray spectrum analysis code. The result of calculated photopeak count and its error are shown in Table 3. For accuracy reasons, only photopeaks with errors of less than 1 % will be considered as radioactive monitors to calculate the reaction rates. The experiment results showed that the standard deviation for the dosimeter sets with Cd foil uncovered and with Cd foil cover on were within (0.02 %-0.99 %) and (0.28 %-0.94 %), respectively.

Reaction rate

The reaction rates of the dosimeters were calculated based on formula (2). Several correction factors should be calculated to obtain the reaction rate value. The neutron self-shielding factors were evaluated based on formulas (9) and (10). The effective neutron self-shielding factors were evaluated based on the calculated self-shielding factor of each energy group using the following equation:

$$F_{SN} = \frac{\int f(E)\sigma(E)\phi(E)dE}{\int \sigma(E)\phi(E)dE} \qquad (17)$$

where $f(E)$ is the energy-dependent neutron self-shielding factor corresponding to the dosimeter form. The $\sigma(E)$ is the multigroup microscopic cross-section based on JENDL Dosimetry File 99 [12] and $\phi(E)$ is the initial neutron spectrum at their irradiation position.

Neutron self-shielding calculations were conducted when dosimeter the material consists of pure metal or alloy. The calculation results indicate that the effect of neutron self-shielding to the reaction rates is less than 0.55 %.

Gamma ray self-absorption correction factors were considered for either dosimeter material itself or vanadium material. For Np and Sc encapsulated by 0.031 cm-thick vanadium capsule, the gamma ray self-absorption correction factors were only considered for the vanadium capsule because of its thickness. However, this assumption may not give so much underestimation despite of the uncertainty of the geometry and physical form of dosimeter material inside the capsule. The gamma ray self-absorption correction factors of dosimeter sets were within (94.97-99.99) %.

The result of burnup correction factor is shown to be within (97.32-100.65) %. Only the burnup correction factor of ^{237}Np fission product is less than one due to the burnt-in effect of higher actinides such as ^{238}Np and ^{238}Pu produced by ^{237}Np (n,γ) reaction. Using the calculated burnup correction factors and neutron self-shielding correction factors, the measured reaction rates were corrected and the results are shown in Table 4. The maximum error was 4.87 % for the ^{237}Np(n,f) reaction.

Table 4. Corrected reaction rates, dosimeter sets, and measured Cd ratio

Reaction Type	Measured Reaction Rate × 10²⁴ (reactions s⁻¹ atom⁻¹ per 100 MWt) (± %ε)		Cd Ratio
	With Cd Covered Dosimeter Set	Without Cd covered Dosimeter Set	
^{59}Co (n,γ) ^{60}Co	9.60×10¹² (2.21)	1.85×10¹³ (2.22)	1.92
^{237}Np (n,f) ^{95}Zr-^{103}Ru	9.90×10¹⁰ (4.77)	1.21×10¹¹ (4.77)	1.22
^{46}Sc (n,γ) ^{46}Sc	1.54×10¹² (2.42)	7.35×10¹² (2.39)	4.76
^{58}Fe(n,γ)^{59}Fe	1.42×10¹¹ (2.87)	4.18×10¹¹ (2.81)	2.95
^{58}Ni (n,p) ^{58}Co	5.43×10⁶ (2.28)	5.38×10⁶ (2.30)	0.99
^{181}Ta (n,γ) ^{182}Ta	9.56×10¹³ (2.85)	9.89×10¹³ (2.85)	1.03

The reaction rate calculation needs to treat time-dependent reactor power and several large data sets. This calculation is implemented by the RRATE code. The measured reaction rates for dosimeter sets not Cd-covered were compared to the Cd-covered dosimeter sets, and the results are shown in Table 4. The Cd-covered dosimeter set is convenient to evaluate for the contribution of measured reaction rate of which come from either thermal or non-thermal (epithermal and fast) neutron. This Cd-covered material is also helpful for reducing activities due to impurities. The Cd cover of 0.5 mm thickness will shield the material against thermal neutron with energies of under 0.55 eV to as low as 1/2500 [44]. The measured Cd ratio of ^{237}Np (n,f), ^{181}Ta (n,γ), and ^{58}Ni (n,p) reactions were obtained as within 0.99-1.22, and those of ^{60}Co (n,γ) and ^{58}Fe (n,γ) were 1.92 and 2.95, respectively. Only ^{45}Sc (n,γ) reaction shows a higher Cd ratio as much as 4.76. It was seen that the Cd ratio is dependent on the span of sensitivity to reaction cross-section window of dosimeter material. From the analysis above, it is concluded that neutron spectrum at the M3 manhole at Z=0.0 mm of elevation from core midplane level was dominated by low-energy neutrons.

Neutron flux

The neutron spectrum at the point where dosimeter sets had been irradiated, was adjusted using NEUPAC, which is a J1-log type spectrum unfolding package. The other required input data are a priori information such as initial spectrum and cross-section data and its covariance. The initial spectrum was calculated using the two-dimensional R-Z and X-Y ordinate discrete transport code DORT. The sets of initial spectrum at the points, where dosimeter sets were irradiated (R=207 cm, Z=0.0 cm from the core mid plane) was used as the guessing spectrum with estimated error of 30 %. Based on DORT calculation the total flux at the irradiation position is 2.10×10^{12} n cm^{-2} s^{-1}, and its neutron spectra are shown in Fig. 4.

The neutron spectra for the dosimeter set that was not Cd-covered was unfolded using either normalized or not normalized spectrum. The result of NEUPAC calculation of the dosimeter sets not covered with Cd are shown as follows. The calculated/experimental reaction rate, C/E's, of ^{59}Co (n,γ) ^{60}Co, ^{237}Np (n,f) ^{95}Zr-^{103}Ru, ^{45}Sc (n,γ) ^{46}Sc, ^{58}Fe (n,γ) ^{59}Fe and ^{181}Ta (n,γ) ^{182}Ta reactions were within 0.05-0.07 in case of using normalized spectrum and sigma test failed. Only C/E of ^{58}Ni (n,p) ^{58}Co reaction type was found to be approximately 1. This reaction was passed the sigma test. But the probability of the spectrum became zero.

On the other hand, if dosimeter sets were evaluated using non-normalized spectrum it was shown that the C/E values of ^{59}Co (n,γ) ^{60}Co, ^{237}Np (n,f) ^{95}Zr-^{103}Ru, ^{45}Sc (n,γ) ^{46}Sc, ^{58}Fe (n,γ) ^{59}Fe, and ^{181}Ta (n,γ) ^{182}Ta reactions were obtained to be approximately 1 and passed the sigma test. However, the ^{58}Ni (n,p) ^{58}Co reaction showed greater than 20 C/E values. The sigma test failed for this reaction and the probabilities of unfolded spectra were very low. In order to confirm that this result comes from either the error of ^{58}Ni (n,p) ^{58}Co reaction rate measurement or a wrong initial spectrum in fast energy region, which was deviated, the investigations were also carried out by removing the ^{58}Ni (n,p) ^{58}Co reaction rate from reaction rate sets input data of NEUPAC adjustment. The result shows that the C/E of reaction rates were 0.95-1.20 and the unfolded neutron spectrum shows reasonable value. The same results were obtained for all the positions and the deviation of C/E value of ^{58}Ni (n,p) ^{58}Co reaction rate from others was constant regardless of the dosimeter sets.

From these results, it can be concluded that the discrepancy of ^{58}Ni (n,p) ^{58}Co reaction rate was due to higher initial spectrum in fast energy region. The initial neutron flux should be reduced to certain amount until the C/E value reaches around 1 before unfolding. Even though the 90 % sensitivity of ^{58}Ni (n,p) ^{58}Co was obtained within 1-6 MeV, its does

not mean that the neutron flux should be reduced only in this region. The reduction of initial spectrum was carried out from fast energy region to the highest upper energy of 90 % confidence level of other reaction type so as not to affect the unfolding result of other reaction rates. This highest upper energy is as much as ~ 1.0×10^{-3} MeV which is from ^{237}Np (n,f) reaction. The biasing processes were conducted by trial and error.

Some efforts were also made to use the neutron flux at 210 through 300 cm points from center core line, which had lower neutron spectrum than that of M3 position, but the unfolded spectrum has not given an acceptable spectrum yet. Finally, the reasonable spectrum was obtained by multiplying 0.01 as a reduction factor from fast energy region which increased gradually to 1 in the intermediate neutron energy region. The bias factor to the DORT initial spectrum is plotted in Fig. 3. The highest upper energy of 90 % confidence level is located approximately at 2.0×10^{-3} MeV. The results of biased initial neutron spectrum, compared to the initial neutron spectrum calculated by DORT for Z=0.0 cm of irradiation position, are shown in Fig. 4.
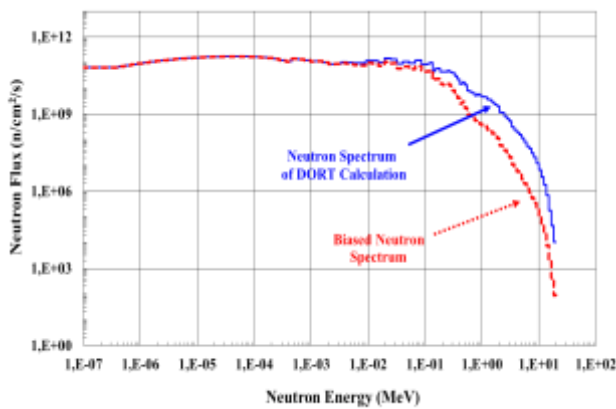

Fig. 4. Initial neutron spectrum by DORT calculation and its biased neutron spectrum.

Here, it can be also concluded that the DORT code needs correction in the fast energy neutron spectrum when it is used out of the core region such as in M3 manhole. It was considered that the bias factor relates to geometry, homogeneity of neutron source, and fission spectrum, since DORT calculation is based on the simplification of geometry and homogeneous core. The biggest correction factor had been shown in the fast neutron energy, and gradually reduced until in epithermal region.

The biased initial neutron spectrum then was used to unfold neutron spectrum for Cd uncovered dosimeter sets. The results of unfolded neutron

spectrum are as follows. The biased initial neutron spectrum, the unfolded neutron spectrum, and the improvement ratio are shown in Fig. 5. This figure also shows the spectrum ratio that is defined as the ratio of initial spectrum from biased DORT calculation to final spectrum. The improvement ratio of each group flux indicates the relative error ratio of input spectrum to the final spectrum. The 90 % confidence interval of ^{59}Co (n,γ) ^{60}Co, ^{45}Sc (n,γ) ^{46}Sc, ^{58}Fe (n,γ) ^{59}Fe, ^{237}Np (n,f) ^{95}Zr-^{103}Ru, and ^{181}Ta (n,γ) ^{182}Ta reactions spans from thermal neutron energy to the intermediate energy. Only the span of the 90 % confidence interval of ^{58}Ni (n,p) ^{58}Co reaction was in the fast neutron energy.
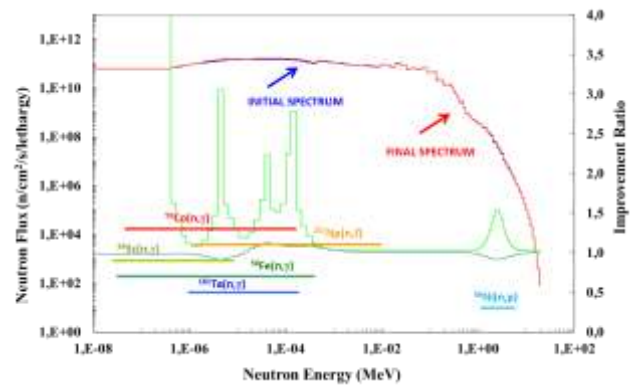

Fig. 5. Unfolded neutron spectrum and improvement ratio of biased calculated spectrum.

The calculated and measured reaction rates of the dosimeter sets without Cd cover were within 0.93-1.04 as is shown in Table 5. The comparison of measured and calculated reaction rates of without Cd covered dosimeter sets after unfolding was shown in Table 6. It was obtained that the C/Es of reaction rates of without Cd covered dosimeters were found to be approximately 0.99-1.04. The adjusted neutron spectrum by NEUPAC was increased the spectrum probability from 99.2 % to the 99.9 %. Table 7 shows final 90 % confidence level of each reaction rate dosimeter sets.

Table 5. Comparison of measured and calculated reaction rates before unfolding

Reaction Type	Reaction Rate $\times 10^{24}$ (reactions s^{-1} atom^{-1} per 100 MWt)			Proba bility (%)
	Experiment	Calculation	C/E	
^{59}Co(n,γ)^{60}Co	1.85×10^{13} (4.12)	1.89×10^{13} (18.82)	1.02 (19.27)	
^{237}Np (n,f)^{95}Zr-^{103}Ru	1.21×10^{11} (5.90)	1.32×10^{11} (18.20)	1.09 (19.13)	
^{45}Sc(n,γ)^{46}Sc	7.35×10^{12} (4.21)	7.20×10^{12} (25.60)	0.98 (25.94)	99.2
^{58}Fe(n,γ)^{59}Fe	4.18×10^{11} (4.47)	4.36×10^{11} (23.23)	1.04 (23.65)	
^{58}Ni (n,p)^{58}Co	5.38×10^{6} (4.16)	5.02×10^{6} (17.31)	0.93 (17.80)	
^{181}Ta(n,γ)^{182}Ta	9.89×10^{13} (4.49)	9.51×10^{13} (19.11)	0.96 (19.63)	

Note: ( )* is % error.

Table 6. Comparison of measured and calculated reaction rates after unfolding

Reaction Type	Reaction Rate × 10^{24} (reactions s^{-1} atom^{-1} per 100 MWt)			Probability (%)
	Experiment	Calculation	C/E	
^{59}Co(n,γ)^{60}Co	$1.85×10^{13}$ (4.12)	$1.84×10^{13}$ (4.07)	1.00 (5.79)	
^{237}Np (n,f)^{95}Zr-^{103}Ru	$1.21×10^{11}$ (5.90)	$1.22×10^{11}$ (6.89)	1.01 (9.07)	
^{45}Sc(n,γ)^{46}Sc	$7.35×10^{12}$ (4.21)	$7.32×10^{12}$ (4.32)	1.00 (6.03)	99.9
^{58}Fe(n,γ)^{59}Fe	$4.18×10^{11}$ (4.47)	$4.35×10^{11}$ (11.32)	1.04 (12.17)	
^{58}Ni (n,p)^{58}Co	$5.38×10^{6}$ (4.16)	$5.37×10^{6}$ (4.09)	1.00 (5.84)	
^{181}Ta(n,γ)^{182}Ta	$9.89×10^{13}$ (4.49)	$9.81×10^{13}$ (6.34)	0.99 (7.77)	

Note: ( )* is % error.

Table 7. 90 % confidence level of each reaction type of no Cd Covered dosimeter set

Reaction Type	Lower Energy (MeV)	Upper Energy (MeV)
^{59}Co(n,γ)^{60}Co	$4.79×10^{-8}$	$1.61×10^{-4}$
^{237}Np (n,f)^{95}Zr-^{103}Ru	$1.29×10^{-6}$	$9.58×10^{-3}$
^{45}Sc(n,γ)^{46}Sc	$2.65×10^{-8}$	$8.10×10^{-6}$
^{58}Fe(n,γ)^{59}Fe	$3.26×10^{-8}$	$3.85×10^{-4}$
^{58}Ni (n,p)^{58}Co	1.18	5.73
^{181}Ta(n,γ)^{182}Ta	$9.80×10^{-7}$	$1.83×10^{-4}$

The result of calculated neutron flux, integral quantity before and after unfolding process, and its error contribution of dosimeter sets were described in Table 8. The total neutron flux, neutron fluxes above 1.0 MeV, neutron flux above 0.1 MeV and displacement rate were $1.75×10^{12}$ n cm^{-2} s^{-1}, $1.83×10^{8}$ n cm^{-2} s^{-1}, $2.94×10^{10}$ n cm^{-2} s^{-1}, and $2.39×10^{-11}$ dpa s^{-1}, respectively. Based on the NEUPAC calculation, the major error contribution to the final unfolded neutron spectra was the error of the initial spectrum.

Table 8. Unfolded neutron spectrum and its integral quantity

Window Function Type	Initial Integral Quantity	Final Integral Quantity	Error (%)	Improvement Ratio
Total Flux	$1.78×10^{12}$	$1.75×10^{12}$	5.17	2.14
> 1.0 MeV	$1.74×10^{8}$	$1.83×10^{8}$	16.80	1.28
> 0.1 MeV	$2.94×10^{10}$	$2.94×10^{10}$	18.92	1.02
Disp. Rate	$2.40×10^{-11}$	$2.39×10^{-11}$	15.31	1.03

Neutron fluence

The dosimeter sets were irradiated in the 35th duty cycle for $4.16×10^{6}$ seconds. Based on its irradiation time, the total fluence and its integral quantities were calculated and the results are as follows. The total fluence, fluence above 1.0 MeV, fluence above 0.1 MeV, and the displacement per atom of dosimeter sets are $7.3×10^{18}$ n cm^{-2},

$7.61×10^{14}$ n cm^{-2}, $1.22×10^{17}$ n cm^{-2}, and $9.96×10^{-5}$ dpa, respectively. The neutron spectrum at M3 in the core mitplane was dominated by soft spectra.

CONCLUSION

The reactor dosimetry test was carried out in the M3 ex-vessel irradiation hole to determine the neutron flux with spectral information. Two dosimeter sets with Cd cover and without Cd cover are loaded to Al capsules and placed at a core midplade level of 207 cm radial distance from core centerline and were irradiated during the 35th cycle of MK-II Joyo. Both dosimeter sets consist of high-purity Co-Al, Sc, Fe, Np, Nb, Ni, B, and Ta. The irradiated dosimeter materials were measured by means of 63-cc HPGe SSD and their gamma-ray spectra were analyzed using BOB75 code. The reaction rates of dosimeters were analyzed based on ^{59}Co (n,γ) ^{60}Co, ^{237}Np (n,f) ^{95}Zr-^{103}Ru, ^{45}Sc (n,γ) ^{46}Sc, ^{58}Fe (n,γ) ^{59}Fe, ^{181}Ta (n,γ) ^{182}Ta, and ^{58}Ni (n,p)^{58}Co reactions. Measured Cd ratios showed that the neutron spectra at the M3 irradiation hole positions were dominated by low-energy neutrons. The neutron flux at irradiated positions was unfolded with measured reaction rates and using initial spectrum of DORT calculation. The experimental validation results show that neutron spectra calculated by DORT need correction for ex-vessel irradiation hole position especially at the fast region. Calculated neutron flux was biased to reduce gradually neutron flux from fast energy region to the intermediate energy to obtain reasonable unfolding result consistent with reaction rate measurement without any exception. Using biased initial spectrum, the neutron flux was estimated by NEUPAC code. The total neutron flux, flux above 1.0 MeV, flux above 0.1 MeV, and its displacement rate dosimeter sets were $1.75×10^{12}$ n cm^{-2} s^{-1}, $1.83×10^{8}$ n cm^{-2} s^{-1}, $2.94×10^{10}$ n cm^{-2} s^{-1}, and $2.39×10^{-11}$ dpa s^{-1}, respectively, with error in estimates were found to be mainly due to the error of the initial spectrum. Results show that the C/E by the ex-vessel neutron dosimetry experiment within 0.99-1.04 with an errors of (5.79-12.17) % for each reaction type, which means these analyses satisfy the acceptable criteria of less than 20 %. This results show that an ex-vessel dosimetry measurement alone give very meaningful result for compensating for in-vessel surveillance capsule whenever dificulties occur in puting dosimeter sets in the inner part of reactor vessel.

ACKNOWLEDGMENT

REFERENCES

1. M.R. Halstead, S. Lee, J. Petrosky *et al.*, Phys. Proc. **26** (2012) 188. doi: 10.1016/j.phpro.2012.03.024

2. M.R. Mitev, S.I. Belousov, K.D. Ilieva *et al.*, Nucl. Eng. Des. **281** (2015) 1. doi:10.1016/j.nucengdes.2014.10.017

3. S. Maeda, H. Naito, C. Ito *et al.,* Prog. Nucl. Sci. Tech. **1** (2011) 182.

4. S. Lee and C. Yoo, J. Kor. Phys. Soc. **59** (2011) 2067.

5. R. Pittarello, A. Vasiliev, H. Ferroukhi *et al.*, Ann. Nucl. Energy **38** (2011) 1842. doi:10.1016/j.anucene.2011.05.017

6. A.B. Tigliole, A. Cammi, D. Chiesa *et al.*, Prog. Nucl. Energy **70** (2014) 249. doi:10.1016/j.pnucene.2013.10.001

7. S.I. Kim, I. Chang, B.H. Kim *et al.*, Nucl. Eng. Tech. **46** (2014) 273. doi:org/10.5516/NET.08.2013.029

8. S.R. Malkawi, B. Khuwaileh and M. Al-Momani, Ann. Nucl. Energy **56** (2013) 17. doi:10.1016/j.anucene.2012.12.025

9. M.A. Lucatero, J.C. Palacios-Hernández, J.O. Villafuerte *et al.*, Nucl. Eng. Des. **240** (2010) 1271. doi:10.1016/j.nucengdes.2010.02.016

10. A. Khajeali, A.R. Farajollahi, R. Khodadadi *et al.*, Appl. Radiat. Isot. **103** (2015) 72. doi:10.1016/j.radphyschem.2015.03.025

11. G. Gambarini, E. Artuso, D. Giove *et al.*, Appl. Radiat. Isot. **106** (2015) 145. doi:10.1016/j.apradiso.2015.07.036

12. S. Jakhar, S. Tiwaria, M. Abhangia *et al.*, Fus. Eng. Des. **100** (2015) 619. doi:10.1016/j.fusengdes.2015.08.015.

13. L. Viererbl, V. Klupak, Z. Lahodova *et al.*, Appl. Radiat. Isot. **70** (2012) 1313. doi:10.1016/j.apradiso.2011.11.032

14. A. Konefał, A. Orlef and M. Bieniasiewicz, Radiat. Meas. **86** (2016) 8. doi:10.1016/j.radmeas.2015.12.039

15. N. Fomin, G.L. Greene, R.R. Allen *et al.*, Nucl. Instrum. Methods. Phys. Res., Sect. **A 773** (2015) 45. doi: 10.1016/j.nima.2014.10.042

16. H. Yucel, I. Cobanbas, A. Kolbas *et al.*, Nucl. Eng. Tech. **48** (2015) 1. doi:10.1016/j.net.2015.11.003

17. O.K. Chopra and A.S. Rao, J. Nucl. Mater. **412** (2011) 195. doi:10.1016/j.jnucmat.2011.02.059

18. M. Ohta, S. Sato, K. Ochiai *et al.*, Fusion Eng. Des. **98–99** (2015) 1847. doi:10.1016/j.fusengdes.2015.03.032

19. E.A. Kenik and J.T. Busby, Mat. Sci. Eng. R. **73** (2012) 67. doi:10.1016/j.mser.2012.05.002

20. S. Sahin and A. Saeed, Ann. Nucl. Energy **89** (2016) 90. doi:10.1016/j.anucene.2015.11.019

21. F. Chen, X. Tang, Y. Yang *et al.*, Nucl. Instrum. Methods Phys. Res., Sect. B **358** (2015) 88. doi:org/10.1016/j.nimb.2015.05.042

22. O.K. Chopra and A.S. Rao, J. Nucl. Mater. **409** (2011) 235. doi:10.1016/j.jnucmat.2010.12.001

23. B. Richardson, C.H. Castano, J. King *et al.*, Nucl. Eng. Des. **245** (2012) 55. doi:10.1016/j.nucengdes.2012.01.023

24. S.R. Malkawi, B. Khuwaileh and M. Al-Momani, Ann. Nucl. Energy **56** (2013) 17. doi:org/10.1016/j.anucene.2012.12.025

25. S. Maeda, H. Naito, C. Ito *et al.*, Prog. Nucl. Sci. Tech. **1** (2011) 182.

26. A. Ballesteros, L. Debarberis, W. Voorbraak *et al*, Prog. Nucl. Energy **52** (2010) 615.

27. G. Aliberti, G. Palmiotti, M. Salvatotes *et al.*, Ann. Nucl. Energy **33** (2006) 700. doi:10.1016/j.anucene.2006.02.003

28. V. Radulović, Ž. Štancar, L.Snoj *et al.*, Appl. Radiat. Isot. **84** (2014) 57. doi:10.1016/j.apradiso.2013.11.027

29. L. Snoja, A. Trkova, R. Jaćimovićc *et al.*, Appl. Radiat. Isot. **69** (2011) 136. doi:10.1016/j.apradiso.2010.08.019

30. M. Angelonea, U. Fischerb, D. Flamminia *et al.,* Fusion Eng. Des. **96–97** (2015) 2. doi:10.1016/j.fusengdes.2015.06.114

31. G. Dobmann, C. Boller, H.G. Herrmann *et al.*, Jap. Soc. Maint., J. Adv. Maint. **5** (2013) 15.

32. M.H. Parajon, E. Abad and F.J. Bermejo, Physics Procedia **60** (2014) 74. doi: 10.1016/j.phpro.2014.11.012.

33. Y.H. Choi and H.G. Joo, J. Nucl. Mater. **426** (2012) 16. doi:0.1016/j.jnucmat.2012.04.002

34. S. Maeda, C. Ito, Y. Ohkawachi *et.al.*, *Characterization of Neutron Fields in the Experimental Fast Reactor Joyo*, Proceedings of the 13th International Symposium on Reactor Dosimetry (2008) 474.

35. T. Aoyama, C. Ito and S. Suzuki, *Current Status and Upgrading Activity of Reactor Material Dosimetry in the Experimental Fast Reactor Joyo*, Proceedings 9th International Symposium on Reactor Dosimetry (1996) 302.

36. S.A. Santa, J. Nucl. Reactor Tech. **11** (2009) 36. (in Indonesian)

37. C. Chilian, R. Chambon and G. Kennedy, Nucl. Instrum. Methods Phys. Res., Sect. A **622** (2010) 429. doi:10.1016/j.nima.2010.01.042.

38. A. Trkova, G. Zerovnika, C. Destouchesb *et al.*, Nucl. Eng. Des. **246** (2012) 69. doi:10.1016/j.nucengdes.2011.06.039

39. H. Soodak, Reactor Handbook Vol. III Part A, Physics, Interscience Publ., New York (1962).

40. C.R. Hammon, The Elements – Handbook of Chemestry and Physcs, 45th ed., The Chemical Rubber Co., Cleveland (1964).

41. T. Kajimoto, S. Endo, N.T. Thanh *et al.*, Appl. Radiat. Isot. **95** (2015) 53. doi:10.1016/j.apradiso.2014.09.018

42. A. Azbouche, M. Belgaid and H. Mazrou, J. Environ. Radioact. **146** (2015) 119. doi: 10.1016/j.jenvrad.2015.04.015

43. K. Kobayashi, T. Iguchi, S. Iwasaki *et al.*, JENDL Dosimetry File 99, JAERI 1344 (2002).

44. Anonymous, *Standard Test Method for Determining Thermal Neutron Reaction and Fluence Rate by Radioactivation Techniques*, Annual Book of ASTM Standards Vol. 12.2, ASTM E-262-13 (2013).